

# ” $\gamma + Jet$ ” process application for setting the absolute scale of jet energy and determining the gluon distribution at the LHC.

D. Bandurin, V. Konoplyanikov, N. Skachkov  
*Joint Institute for Nuclear Research, Dubna, Russia*

## Abstract

The possibility of jet energy scale setting at the CMS calorimeter by using ” $\gamma + Jet$ ” process is studied. The estimation of the number of ” $\gamma + Jet$ ” events suitable for determination of gluon distribution inside a proton in a new kinematic region of  $x$ ,  $Q^2$  variables beyond the one covered by HERA data is also presented.

## 1. Introduction.

Basing on the selection criteria introduced for the first time in [1]–[4] (see below Section 2), the background events suppression factors, signal events selection efficiencies and the number of the events, that can be collected at integrated luminosity  $L_{int} = 3 \text{ fb}^{-1}$  are determined here.

It is also shown that ” $\gamma + Jet$ ” events, being collected at LHC, would provide us with the data sufficient for an extraction of gluon distribution function in a proton. A new region of  $2 \cdot 10^{-4} \leq x \leq 1$  and  $1.6 \cdot 10^3 \leq Q^2 \leq 8 \cdot 10^4 \text{ (GeV/c)}^2$  can be covered. The rates of  $g c \rightarrow \gamma^{dir} + Jet$  events are also given.

## 2. Definition of selection cuts for physical variables and the scalar form of the $P_t$ balance equation.

1. We shall select the events with one jet and one “ $\gamma^{dir}$ -candidate” (in what follows we designate it as  $\gamma$  and call the “photon” for brevity and only in Section 3, devoted to the backgrounds, we denote  $\gamma^{dir}$ -candidate by  $\tilde{\gamma}$ ) with

$$P_t^\gamma \geq 40 \text{ GeV}/c \quad \text{and} \quad P_t^{Jet} \geq 30 \text{ GeV}/c. \quad (1)$$

The electromagnetic calorimeter (ECAL) signal can be considered as a candidate for a direct photon if it fits inside the  $5 \times 5$  ECAL crystal cell window having a cell with the highest  $P_t \gamma/e$  in the center ([6]).

The jet is defined here according to the PYTHIA [7] jetfinding algorithm LUCCELL. The jet cone radius  $R$  in the  $\eta - \phi$  space counted from the jet initiator cell (ic) is taken to be  $R_{ic} = ((\Delta\eta)^2 + (\Delta\phi)^2)^{1/2} = 0.7$ .

2. To suppress the background processes, i.e. to select mostly the events with “isolated” photons and to discard the events with fake “photons” (that may originate as “ $\gamma^{dir}$ -candidates” from meson decays, for instance), we restrict

a) the value of the scalar sum of  $P_t$  of hadrons and other particles surrounding a “photon” within a cone of  $R_{isol}^\gamma = ((\Delta\eta)^2 + (\Delta\phi)^2)^{1/2} = 0.7$  (“absolute isolation cut”)

$$\sum_{i \in R} P_t^i \equiv P_t^{isol} \leq P_{tCUT}^{isol}; \quad (2)$$

b) the value of a fraction (“relative isolation cut”)

$$\sum_{i \in R} P_t^i / P_t^\gamma \equiv \epsilon^\gamma \leq \epsilon_{CUT}^\gamma. \quad (3)$$

3. To be consistent with the application condition of the NLO formulae, one should avoid an infrared dangerous region and take care of  $P_t$  population in the region close to a  $\gamma^{dir}$ -candidate we also restrict in accordance with [8] and [9] the scalar sum of  $P_t$  of particles around a “photon” within a cone of a smaller radius  $R_{singl}^\gamma = 0.175 = 1/4 R_{isol}^\gamma$ :

$$\sum_{i \in R_{singl}^\gamma} P_t^i \equiv P_t^{singl} \leq 2 \text{ GeV}/c \quad (i \neq \gamma - dir). \quad (4)$$

4. We accept only the events having no charged tracks (particles) with  $P_t > 1 \text{ GeV}/c$  within the  $R_{singl}^\gamma$  cone around the  $\gamma^{dir}$ -candidate.

5. To suppress the background events with photons resulting from high-energy  $\pi^0$ ,  $\eta$ ,  $\omega$  and  $K_S^0$  meson decays, we require the absence of a high  $P_t$  hadron in the calorimeter tower containing the  $\gamma^{dir}$ -candidate:

$$P_t^{hadr} \leq 5 \text{ GeV}/c. \quad (5)$$

At the PYTHIA level of simulation this cut may effectively take into account the imposing of an upper cut on the hadronic calorimeter (HCAL) signal in the towers behind the ECAL tower fired by the direct photon.

6. We select the events with the vector  $\vec{P}_t^{Jet}$  being “back-to-back” to the vector  $\vec{P}_t^\gamma$  (in the plane transverse to the beam line) within  $\Delta\phi$  defined by the equation:

$$\phi_{(\gamma, jet)} = 180^\circ \pm \Delta\phi \quad (\Delta\phi = 15^\circ, 10^\circ, 5^\circ) \quad (6)$$

( $5^\circ$  is one HCAL tower size in  $\phi$ ), where  $\phi_{(\gamma, jet)}$  is the angle between the  $P_t^\gamma$  and  $P_t^{Jet}$  vectors:  $\vec{P}_t^\gamma \vec{P}_t^{Jet} = P_t^\gamma P_t^{Jet} \cdot \cos(\phi_{(\gamma, jet)})$ , where  $P_t^\gamma = |\vec{P}_t^\gamma|$ ,  $P_t^{Jet} = |\vec{P}_t^{Jet}|$ .

7. The initial and final state radiations (ISR and FSR) manifest themselves most clearly as some final state mini-jets or clusters activity. To suppress it, we impose a new cut condition that was not formulated in an evident form in previous experiments: we choose the ” $\gamma + Jet$ ” events that do not have any other jet-like or cluster high  $P_t$  activity by selecting the events with the values of  $P_t^{clust}$  (the cluster cone  $R_{clust}(\eta, \phi) = 0.7$ ), being lower than some threshold  $P_{tCUT}^{clust}$  value, i.e. we select the events with

$$P_t^{clust} \leq P_{tCUT}^{clust} \quad (7)$$

( $P_{tCUT}^{clust} = 15, 10, 5 \text{ GeV}/c$  are most efficient as will be shown in Section 3). Here, the clusters are found by one and the same jetfinder LUCCELL.

Now we pass to another new quantity (introduced also for the first time in [1]–[4]) that can be measured at the experiment.

8. We limit the value of the modulus of the vector sum of  $\vec{P}_t$  of all particles, except those of the ” $\gamma + Jet$ ” system, that fit into the region  $|\eta| < 5.0$  covered by the ECAL and HCAL, i.e., we limit the signal in the cells “beyond the jet and photon” region by the following cut:

$$\left| \sum_{i \notin Jet, \gamma-dir} \vec{P}_t^i \right| \equiv P_t^{out} \leq P_{tCUT}^{out}, \quad |\eta_i| < 5.0. \quad (8)$$

The importance of  $P_{tCUT}^{out}$  and  $P_{tCUT}^{clust}$  for selection of events with a good balance of  $P_t^\gamma$  and  $P_t^{Jet}$  and for the background reduction will be demonstrated in Section 3.

Below the set of selection cuts 1 – 8 will be referred to as “Selection 1”. The last two of them, 7 and 8, are new criteria [1]–[4] not used in previous experiments. In addition to them one more new object, introduced in [4] and named an “isolated jet”, will be discussed.

9. We also involve a new requirement of “jet isolation”, i.e. the presence of a “clean enough” (in the sense of limited  $P_t$  activity) region inside the ring (of  $\Delta R = 0.3$  or of approximately a size of three calorimeter towers) around the jet. Following this picture, we restrict the ratio of the scalar sum of transverse momenta of particles belonging to this ring, i.e.

$$P_t^{ring} / P_t^{Jet} \equiv \epsilon^{jet}, \quad \text{where} \quad P_t^{ring} = \sum_{i \in 0.7 < R < 1} |\vec{P}_t^i|. \quad (9)$$

( $\epsilon^{jet} \leq 3 - 5\%$ ). The set of events that pass cuts 1 – 9 will be called “Selection 2”.

The exact values of the cut parameters  $P_{tCUT}^{isol}$ ,  $\epsilon_{CUT}^\gamma$ ,  $\epsilon^{jet}$ ,  $P_{tCUT}^{clust}$ ,  $P_{tCUT}^{out}$  will be specified below, since they may be different, for instance, for various  $P_t^\gamma$  intervals (being looser for higher  $P_t^\gamma$ ).

10. One can expect reasonable results of the jet energy calibration procedure modeling and subsequent practical realization only if one uses a set of selected events with small  $P_t^{miss}$  caused by neutrinos instrumental/material features of the detector. So, we also use the following cut:

$$P_t^{miss} \leq P_{tCUT}^{miss}. \quad (10)$$

The aim of the event selection with small  $P_{t(\nu)}^{Jet}$  is quite obvious: we need a set of events with a reduced  $P_t^{Jet}$  uncertainty due to possible presence of a non-detectable neutrino contribution to a jet, for example [4].

To conclude this section, let us rewrite the scalar  $P_t$  balance equation from [4] with the notations introduced there in the form more suitable to present the final results:

$$\frac{P_t^\gamma - P_t^{Jet}}{P_t^\gamma} = (1 - \cos\Delta\phi) + P_t(O + \eta > 5.0)/P_t^\gamma, \quad (11)$$

where  $P_t(O + \eta > 5.0) \equiv (\vec{P}_t^O + \vec{P}_t^{|\eta|>5.0}) \cdot \vec{n}^{Jet}$  with  $\vec{n}^{Jet} = \vec{P}_t^{Jet}/P_t^{Jet}$ . Here  $P_t^O$  is a total transverse momentum of all particles beyond " $\gamma + Jet$ " system in the  $|\eta| < 5.0$  region and  $P_t^{|\eta|>5.0}$  is a total transverse momentum of all particles flying in the direction of a non-instrumented forward part ( $|\eta| > 5.0$ ) of the D0 detector.

As shown in Section [4], the first term on the right-hand side of equation (11), i.e.  $(1 - \cos\Delta\phi)$  is negligibly small and tends to decrease fast with growing  $P_t^{Jet}$ . So, the main contribution to the  $P_t$  disbalance in the " $\gamma + Jet$ " system is caused by the term  $P_t(O + \eta > 5.0)/P_t^\gamma$ .

### 3. Detailed study of background suppression.

To estimate the background for the signal events, we carried out the simulation with a mixture of all QCD and SM subprocesses with large cross sections existing in PYTHIA <sup>1</sup>, namely, ISUB=1, 2, 11–20, 28–31, 53, 68, which can lead to a large background for our main "signal" subprocesses (12) and (13) (ISUB=14 and 29 in PYTHIA) <sup>2</sup>:

<sup>1</sup> PYTHIA 5.7 version with default CTEQ2L parametrisation of structure functions is used here.

<sup>2</sup>A contribution of another possible NLO channel  $gg \rightarrow g\gamma$  (ISUB=115 in PYTHIA) was found to be still negligible even at LHC energies.

“Compton-like” process

$$qg \rightarrow q + \gamma \quad (12)$$

and the “annihilation” process

$$q\bar{q} \rightarrow g + \gamma. \quad (13)$$

Three generations with the abovementioned set of subprocesses were performed, each with different minimal values of  $P_t$  appearing in the final state of the hard  $2 \rightarrow 2$  subprocess, i.e.  $\hat{p}_\perp^{min} = CKIN(3)$  parameter in PYTHIA that practically coincides with  $P_t^\gamma$  in the case of signal direct photons production (compare lines 2 and 3 from the column “ $S$ ” of Table 2). These values were  $\hat{p}_\perp^{min} = 40$   $GeV/c$ , 100 and 200  $GeV/c$ . By 40 million events were generated for three  $\hat{p}_\perp^{min}$  values respectively. The cross sections of the abovementioned subprocesses define the rates of corresponding physical events and, thus, appear here as weight factors.

We selected “ $\gamma^{dir}$ -candidate +1 Jet” events with  $P_t^{Jet} > 30$   $GeV/c$  containing one  $\gamma^{dir}$ -candidate (denoted as  $\tilde{\gamma}$ ) to be identified by the detector as an isolated photon<sup>3</sup> with  $R_{isol}^\gamma = 0.7$  and  $P_t^{\tilde{\gamma}} \geq 40$  ( 100 and 200)  $GeV/c$  for the generation with  $\hat{p}_\perp^{min} = 40$  ( 100 and 200)  $GeV/c$  respectively (see below cut 3  $P_t^{\tilde{\gamma}} \geq \hat{p}_\perp^{min}$  of Table 1.). Here and below, speaking about the  $\gamma^{dir}$ -candidate, we actually mean a signal that may be registered in the  $5 \times 5$  ECAL crystal cell window having the cell with the highest  $P_t$  photon or electron ( $\gamma/e$ ) in its center. All these photon candidates were supposed to satisfy isolation criteria of [4] with the values given in Table 1:  $P_{tCUT}^{isol} = 2$   $GeV/c$  and  $\epsilon_{CUT}^{\tilde{\gamma}} = 5\%$ .

We apply the cuts from Table 1 one after another on the observable physical variables. The influence of these cuts on the signal-to-background ratio  $S/B$  is presented in Tables 2, 5–7.

Tables 2 and 5 are complementary to each other. The numbers in the left-hand column (“Cut”) of Table 2, coincide with the numbers of cuts listed in Table 1.

The second and third columns contain respectively the numbers of signal direct photons ( $S$ )<sup>4</sup> and background  $\gamma^{dir}$ -candidates ( $B$ ) left in the sample of events after application of each cut. The numbers of background events  $B$  do not include events with electrons. Their numbers in the samples are presented

<sup>3</sup>For brevity we denote the direct photon and the “ $\gamma^{dir}$ -candidate” by the same symbol “ $\tilde{\gamma}$ ”.

<sup>4</sup>Their number coincide starting from line 3 of Table 1 with the number of events with (12) and (13) fundamental  $2 \rightarrow 2$  subprocesses of direct photon production.

separately in the last right-hand column “ $e^\pm$ ”. The other columns of Table 2 include efficiencies  $E f f_{S(B)}$  (with their errors) defined as a ratio of the number of signal (background) events that passed under a cut (1–17) to the number of the preselected events (1st cut of this table). They are followed by the column containing the values of  $S/B$  (without account of events with electrons that fake direct photons).

Table 1: List of the applied cuts used in Tables 2, 5–7.

---

<b>0.</b> No cuts;	
<b>1.</b> $P_t^{\tilde{\gamma}} \geq 40 \text{ GeV}/c$ , <b>b)</b> $ \eta^{\tilde{\gamma}}  \leq 2.61$ , <b>c)</b> $P_t^{jet} \geq 30 \text{ GeV}/c$ , <b>d)</b> $P_t^{hadr} < 5 \text{ GeV}/c$ *;	
<b>2.</b> $\epsilon^{\tilde{\gamma}} \leq 15\%$ ;	<b>11.</b> $P_t^{clust} < 20 \text{ GeV}/c$ ;
<b>3.</b> $P_t^{\tilde{\gamma}} \geq \hat{p}_\perp^{min}$ ;	<b>12.</b> $P_t^{clust} < 15 \text{ GeV}/c$ ;
<b>4.</b> $\epsilon^{\tilde{\gamma}} \leq 5\%$ ;	<b>13.</b> $P_t^{clust} < 10 \text{ GeV}/c$ ;
<b>5.</b> $P_t^{isol} \leq 2 \text{ GeV}/c$ ;	<b>14.</b> $P_t^{out} < 20 \text{ GeV}/c$ ;
<b>6.</b> $N_{jet} \leq 3$ ;	<b>15.</b> $P_t^{out} < 15 \text{ GeV}/c$ ;
<b>7.</b> $N_{jet} \leq 2$ ;	<b>16.</b> $P_t^{out} < 10 \text{ GeV}/c$ ;
<b>8.</b> $N_{jet} = 1$ ;	<b>17.</b> $\epsilon^{jet} \leq 5\%$ .
<b>9.</b> $\Delta\phi < 15^\circ$ ;	
<b>10.</b> $P_t^{miss} \leq 10 \text{ GeV}/c$ ;	

---

\*  $P_t$  of a hadron in the 5x5 ECAL cell window containing the  $\gamma^{dir}$ -candidate in the center.

From the first line of Table 14 we see that without imposing any cut the number of background events  $B$  (the 3rd column) exceeds the number of signal events  $S$  (the 2nd column) by 5 orders of magnitude. The relative isolation cut 2 ( $\epsilon^{\tilde{\gamma}} \leq 15\%$ ) makes the  $S/B$  ratio equal to 0.28. Cut 3 ( $P_t^{\tilde{\gamma}} \geq \hat{p}_\perp^{min}$ ) improves the  $S/B$  ratio to 0.71. Relative isolation cut 4 and then the absolute isolation cut 5 make the  $S/B$  ratio to be equal to 1.50 and 1.93, respectively. The requirement of only one jet being present in the event (cut 8) results in the value  $S/B = 5.96$ . The ratio  $S/B$  is increased by the cut  $\Delta\phi < 15^\circ$  to 6.54 (cut 9) and at the same time the number of signal events is decreased only by 5%.

In line 10 we used the  $P_{tCUT}^{miss}$  cut, described in Section 2, to reduce uncertainty of  $P_t^{jet}$  due to a possible neutrino contribution to a jet, for example. It also reduces the contribution to background from the decay subprocesses  $qg \rightarrow q' + W^\pm$  and  $q\bar{q}' \rightarrow g + W^\pm$  with the subsequent decay  $W^\pm \rightarrow e^\pm\nu$  that leads to a substantial  $P_t^{miss}$  value. It is clear from the distributions over  $P_t^{miss}$  for two  $P_t^e$  intervals presented in Fig. 1. From the last column ( $e^\pm$ ) of Table 2 one can see that  $P_{tCUT}^{miss}$  cut (see line 10) reduces strongly (5 times) the number of events containing  $e^\pm$  as direct photon candidates. So,  $P_{tCUT}^{miss}$  would make a noticeable improvement of the total  $S/B$  ratio.

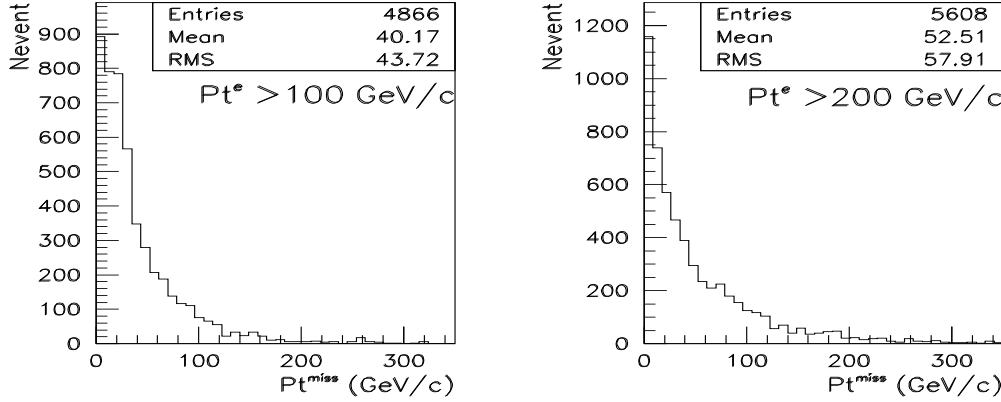


Fig. 1: Distribution of events over  $P_t^{miss}$  in events with energetic  $e^\pm$ 's appearing as direct photon candidates for the cases  $P_t^e \geq 100 \text{ GeV}/c$  and  $P_t^e \geq 200 \text{ GeV}/c$  (here are used events satisfying cuts 1–3 of Table 1).

The cuts 11–13 show step-by-step influence of  $P_t^{clust}$ . The reduction of  $P_t^{clust}$  to  $10 \text{ GeV}/c$  (cut 13) results in significant improvement (about 3 times as compared with line 10) of the  $S/B$  ratio to 17.64. Further reduction of  $P_t^{out}$  to  $10 \text{ GeV}/c$  (cut 16) improves  $S/B$  to 22.67. The jet isolation requirement  $\epsilon^{jet} < 5\%$  (line 17) finally gives  $S/B = 24.46$ <sup>5</sup>. The summary of Table 2 is presented in the middle section ( $\hat{p}_\perp^{min} = 100 \text{ GeV}/c$ ) of Table 5 where line “Preselected” corresponds to the cut 1 of Table 1 and correspondingly to the line number 1 of Table 2 presented above. The line “After cuts” corresponds to the line 16 of Table 2 and line “+jet isolation” corresponds to the line 17.

Tables 3 and 4 show the relative contributions of four main (having the largest cross sections) fundamental QCD subprocesses  $qg \rightarrow qg$ ,  $qq \rightarrow qq$ ,  $gg \rightarrow q\bar{q}$  and  $gg \rightarrow gg$  into production of the background “ $\gamma$ -brem” and “ $\gamma$ -mes” events selected by criteria 1–13 of Table 1 for three  $P_t^\gamma$  intervals. In some lines of Tables 3 and 4 the sum over contributions from the four considered QCD subprocesses is less than 100%. The remained percentages correspond to other subprocesses (like  $q\bar{q} \rightarrow q\bar{q}$ ).

It is useful to note from Tables 3 and 4 that most of background events (85% at least) originate from  $qg \rightarrow qg$  and  $qq \rightarrow qq$  scatterings with an increase of contribution from the last one with growing  $P_t^\gamma$ .

The simulation in PYTHIA also predicts that practically in all selected “ $\gamma$ -brem” events “bremsstrahlung photons” are produced in the final state

<sup>5</sup>Stricter isolation requirement  $\epsilon^{jet} < 2\%$  considered in [4] would lead to  $S/B = 31.1$ .

Table 2: Values of significance and efficiencies for  $\hat{p}_\perp^{min}=100 \text{ GeV}/c$ .

Cut	$S$	$B$	$Eff_S(\%)$	$Eff_B(\%)$	$S/B$	$e^\pm$
0	19420	5356.E+6			0.00	3.9E+6
1	19359	1151425	$100.00 \pm 0.00$	$100.000 \pm 0.000$	0.02	47061
2	18236	65839	$94.20 \pm 0.97$	$5.718 \pm 0.023$	0.28	8809
3	15197	22437	$78.50 \pm 0.85$	$1.949 \pm 0.013$	0.71	2507
4	14140	9433	$73.04 \pm 0.81$	$0.819 \pm 0.008$	1.50	2210
5	8892	4618	$45.93 \pm 0.59$	$0.401 \pm 0.006$	1.93	1331
6	8572	3748	$44.28 \pm 0.57$	$0.326 \pm 0.005$	2.29	1174
7	7663	2488	$39.58 \pm 0.53$	$0.216 \pm 0.004$	3.08	921
8	4844	813	$25.02 \pm 0.40$	$0.071 \pm 0.002$	5.96	505
9	4634	709	$23.94 \pm 0.39$	$0.062 \pm 0.002$	6.54	406
10	4244	650	$21.92 \pm 0.37$	$0.056 \pm 0.002$	6.53	87
11	3261	345	$16.84 \pm 0.32$	$0.030 \pm 0.002$	9.45	53
12	2558	194	$13.21 \pm 0.28$	$0.017 \pm 0.001$	13.19	41
13	1605	91	$8.29 \pm 0.22$	$0.008 \pm 0.001$	17.64	26
14	1568	86	$8.10 \pm 0.21$	$0.007 \pm 0.001$	18.23	26
15	1477	77	$7.63 \pm 0.21$	$0.007 \pm 0.001$	19.18	25
16	1179	52	$6.09 \pm 0.18$	$0.005 \pm 0.001$	22.67	22
17	1125	46	$5.81 \pm 0.18$	$0.004 \pm 0.001$	24.46	21

\* The background ( $B$ ) is considered here with no account of contribution from the “ $e^\pm$  events” in which  $e^\pm$ ’s appear as  $\gamma^{dir}$ -candidates.

of the fundamental subprocess. Namely, they are radiated from the outgoing quarks in the case of the first three subprocesses and appear as the result of string breaking in the case of  $gg \rightarrow gg$  scattering which, naturally, gives a small contribution into “ $\gamma + Jet$ ” events production.

Table 5 shows in more detail the origin of  $\gamma^{dir}$ -candidates photons. So, in Table 5 the numbers in the “ $\gamma - direct$ ” column correspond to the respective numbers of signal events in lines 1, 16 and 17 and column “ $S$ ” of Table 2 while the numbers in the “ $\gamma - brem$ ” column of Table 5 correspond to the numbers of events with the photons radiated from quarks participating in the hard interactions. The total number of background events, i.e. a sum over the numbers presented in columns 4 – 8 in the same line, is shown in the column “ $B$ ” of Table 2. The other lines of Table 5 for  $\hat{p}_\perp^{min} = 40$  and  $200 \text{ GeV}/c$  have the meaning analogous to that described above for  $\hat{p}_\perp^{min} = 100 \text{ GeV}/c$ .

The last column of Table 5 shows the number of events with  $e^\pm$ . In this pa-



Table 3: Relative contribution (in per cents) of different QCD subprocesses into the “ $\gamma$ -*brem*” events production.

$P_t^\gamma$ (GeV/c)	fundamental QCD subprocess			
	$qg \rightarrow qg$	$qq \rightarrow qq$	$gg \rightarrow q\bar{q}$	$gg \rightarrow gg$
40–71	$70.6 \pm 8.7$	$21.1 \pm 3.8$	$5.1 \pm 1.6$	$2.6 \pm 1.0$
71–141	$67.5 \pm 7.3$	$23.6 \pm 3.5$	$4.2 \pm 1.2$	$2.6 \pm 0.9$
141–283	$58.7 \pm 9.0$	$30.7 \pm 5.7$	$1.8 \pm 1.0$	—

Table 4: Relative contribution (in per cents) of different QCD subprocesses into the “ $\gamma$ -*mes*” events production.

$P_t^\gamma$ (GeV/c)	fundamental QCD subprocess			
	$qg \rightarrow qg$	$qq \rightarrow qq$	$gg \rightarrow q\bar{q}$	$gg \rightarrow gg$
40–71	$65.2 \pm 9.9$	$20.1 \pm 4.5$	$7.1 \pm 2.5$	$7.2 \pm 2.3$
71–141	$63.7 \pm 11.6$	$23.0 \pm 5.2$	$7.2 \pm 2.6$	$4.4 \pm 1.4$
141–283	$57.7 \pm 26.2$	$23.1 \pm 13.9$	$7.7 \pm 6.9$	$3.8 \pm 4.6$

per we suppose the 100% track finding efficiency<sup>6</sup> for  $e^\pm$  with  $P_t^e > 40 \text{ GeV}/c$ .

The numbers in Tables 6 and 7 accumulate in a compact form the information of Table 2 and 5. Thus, for example, the columns  $S$  and  $B$  of the middle lines for  $\hat{p}_\perp^{\min} = 100 \text{ GeV}/c$  contain the numbers of the signal and background events taken at the level of line 16 (for Table 6) and line 17 (for Table 7).

From Table 6 it is seen that the ratio  $S/B$  grows while  $P_t^{\tilde{\gamma}}$  increases from 3.9 at  $P_t^{\tilde{\gamma}} \geq 40 \text{ GeV}/c$  to 48.4 at  $P_t^{\tilde{\gamma}} \geq 200 \text{ GeV}/c$ . The jet isolation requirement (cut 17 from Table 1) noticeably improves the situation at low  $P_t^{\tilde{\gamma}}$  (see Table 7). After application of this criterion  $S/B$  increases to 5.1 at  $P_t^{\tilde{\gamma}} \geq 40 \text{ GeV}/c$  and to 24.46 at  $P_t^{\tilde{\gamma}} \geq 100 \text{ GeV}/c$ . Remember the conclusion that the sample of events selected with our criteria has a tendency to contain more events with an isolated jet as  $P_t^{\tilde{\gamma}}$  increases.

So, from Tables 5 – 7 we see that the cuts listed in Table 1 (containing moderate values of  $P_{tCUT}^{\text{clust}}$  and  $P_{tCUT}^{\text{out}}$ ) allow the major part of the background events to be suppressed. The influence of wide variation of these two cuts on

- the number of selected events (for  $L_{\text{int}} = 3 \text{ fb}^{-1}$ );
- the signal-to-background ratio  $S/B$ ;
- the mean values of  $(P_t^{\tilde{\gamma}} - P_t^{\text{Jet}})/P_t^{\tilde{\gamma}}$  and its standard deviation value  $\sigma(F)$

<sup>6</sup>But, certainly, these electrons can be detected with the non-zero probability as a direct photon and their real contribution to the total background  $B$  should be obtained after account of the efficiency of charged tracks determination.

Table 5: Number of signal and background events remained after cuts.

$\hat{p}_\perp^{min}$ (GeV/c)	Cuts	$\gamma$ direct	$\gamma$ brem	photons from the mesons				$e^\pm$
				$\pi^0$	$\eta$	$\omega$	$K_S^0$	
40	Preselected	12394	20952	166821	66533	17464	23942	6684
	After cuts	1718	220	146	56	2	15	10
	+ jet isol.	1003	102	59	26	2	7	8
100	Preselected	19359	90022	658981	247644	69210	85568	47061
	After cuts	1179	34	13	4	1	0	22
	+ jet isol.	1125	32	9	4	1	0	21
200	Preselected	55839	354602	1334124	393880	141053	167605	153410
	After cuts	1838	27	5	5	0	1	17
	+ jet isol.	1831	127	5	5	0	1	17

Table 6: Efficiencies and significance values in events without jet isolation cut.

$\hat{p}_\perp^{min}$ (GeV/c)	$S$	$B$	$Eff_S(\%)$	$Eff_B(\%)$	$S/B$	$S/\sqrt{B}$
40	1718	439	$13.86 \pm 0.36$	$0.149 \pm 0.007$	3.9	82.0
100	1179	52	$6.09 \pm 0.18$	$0.005 \pm 0.001$	22.7	163.5
200	1838	38	$3.29 \pm 0.09$	$0.004 \pm 0.001$	48.4	298.2

Table 7: Efficiencies and significance values in events with jet isolation cut.

$\hat{p}_\perp^{min}$ (GeV/c)	$S$	$B$	$Eff_S(\%)$	$Eff_B(\%)$	$S/B$	$S/\sqrt{B}$
40	1003	196	$8.09 \pm 0.27$	$0.066 \pm 0.005$	5.1	71.6
100	1125	46	$5.81 \pm 0.18$	$0.004 \pm 0.001$	24.5	165.9
200	1831	38	$3.29 \pm 0.09$	$0.004 \pm 0.001$	48.4	298.2

is presented in Tables 1 – 8 of Appendix. Cuts (1) – (10) of Table 1 of this section were applied to select “direct photon candidate + 1 jet” events for the tables of this Appendix. The jets in these events as well as clusters were found by only one LUCCELL jetfinder (for the whole  $\eta$  region  $|\eta^{jet}| < 5.0$ ).

Tables 1 – 4 of Appendix correspond to the simulation with  $\hat{p}_\perp^{min} = 40$  GeV/c and Tables 5 – 8 to that with  $\hat{p}_\perp^{min} = 200$  GeV/c. The rows and columns of Tables 1 – 8 illustrate the influence of  $P_{tCUT}^{clust}$  and  $P_{tCUT}^{out}$  on the quantities mentioned above (in the points (a), (b), (c)).

First of all, we see from Tables 2 and 6 of Appendix that a noticeable reduction of the background take place while moving along the diagonal from

the right-hand bottom corner to the left-hand upper one, i.e. with reinforcing  $P_{tCUT}^{clust}$  and  $P_{tCUT}^{out}$ . So, we see that for  $\hat{p}_{\perp}^{min} = 40 \text{ GeV}/c$  the ratio  $S/B$  changes in the table cells along the diagonal from  $S/B = 2.3$  (in the case of no limits on these two variables), to  $S/B = 3.9$  for the cell with  $P_{tCUT}^{clust} = 10 \text{ GeV}/c$  and  $P_{tCUT}^{out} = 10 \text{ GeV}/c$ . Analogously, for  $\hat{p}_{\perp}^{min} = 200 \text{ GeV}/c$   $S/B$  changes for the same table cells from 13.6 to 48.4 (see the figures in Table 6 of Appendix).

The second observation. The restriction of  $P_{tCUT}^{clust}$  and  $P_{tCUT}^{out}$  improves the calibration accuracy. Table 3 of Appendix shows that the mean value of the fraction  $F \equiv (P_t^{\tilde{\gamma}} - P_t^{Jet})/P_t^{\tilde{\gamma}}$  decreases from 0.030 (the bottom right-hand corner) to 0.009 for  $P_{tCUT}^{clust} = 10 \text{ GeV}/c$  and  $P_{tCUT}^{out} = 10 \text{ GeV}/c$ . Simultaneously, by this restriction one noticeably decreases (about a factor of two: from 0.163 to 0.085 for  $\hat{p}_{\perp}^{min} = 40 \text{ GeV}/c$ , for instance) the width of the gaussian  $\sigma(F)$  (see Tables 4 and 8 of Appendix).

The explanation is simple. The balance equation (11) contains 2 terms on the right-hand side  $(1 - \cos\Delta\phi)$  and  $P_t(O + \eta > 5.0)/P_t^{\tilde{\gamma}}$ . The first one is negligibly small and tends to decrease with growing  $P_t^{\tilde{\gamma}}$  (see [4] for details). So, we see that the main source of the disbalance in equation (11) is the term  $P_t(O + \eta > 5.0)/P_t^{\tilde{\gamma}}$ . This term can be decreased by decreasing  $P_t$  activity beyond the jet.

Thus, we can conclude that application of two criteria introduced in Section 2, i.e.  $P_{tCUT}^{clust}$  and  $P_{tCUT}^{out}$ , results in two important consequences: significant background reduction and essential improvement of the calibration accuracy.

The numbers of events (for  $L_{int} = 3 \text{ fb}^{-1}$ ) for different  $P_{tCUT}^{clust}$  and  $P_{tCUT}^{out}$  are given in the cells of Tables 1 and 5 of Appendix. One can see that even with such strict  $P_{tCUT}^{clust}$  and  $P_{tCUT}^{out}$  values as  $10 \text{ GeV}/c$  for both, for example, we would have a sufficient number of events (about 3 600 000 for  $P_t^{\tilde{\gamma}} \geq 40 \text{ GeV}/c$ , and 4 000  $P_t^{\tilde{\gamma}} \geq 200 \text{ GeV}/c$ ) with low background contamination ( $S/B = 3.9$  and 48.4 for  $P_t^{\tilde{\gamma}} \geq 40 \text{ GeV}/c$  and  $P_t^{\tilde{\gamma}} \geq 200 \text{ GeV}/c$  respectively) and a good accuracy of the absolute jet energy scale setting.

Let us mention that all these PYTHIA results can serve as preliminary ones and only full GEANT simulation would allow one to come to a final conclusion.

To conclude this section we would like to stress that, as is seen from Table 5, the “ $\gamma - brem$ ” background defines a dominant part of the total background. Its contribution is about the same (see Table 5) as the combined background contribution from neutral meson decays. We would like to emphasize here that this is a strong prediction of PYTHIA generator which has to be compared with predictions of other generator like HERWIG, for example.

Secondly, we would like to underline also that as it is seen from Table 14, 17 the photon isolation and selection cuts 1–5, usually used in the study of inclusive photon production, increase the  $S/B$  ratio up to 1.93 only while the other cuts 6–17, that select events with a clear “ $\gamma + Jet$ ” topology and limited  $P_t$  activity beyond a chosen single jet, lead to a significant improvement of  $S/B$  by about one order of magnitude to 24.46.

The numbers in the tables of Appendix were obtained with inclusion of the contribution from the background events. The tables show that they account does not spoil the  $P_t^\gamma - P_t^{Jet}$  balance. The estimation of the number of these background events would be important for the gluon distribution determination (see Section 4).

#### 4. “ $\gamma + Jet$ ” event rate estimation for gluon distribution determination at the LHC.

As many of theoretical predictions for production of new particles (Higgs, SUSY) at the LHC are based on model estimations of the gluon density behavior at low  $x$  and high  $Q^2$ , measurement of the proton gluon density for this kinematic region directly in LHC experiments would be obviously useful. One of the promising channels for this measurement, as was shown in [10], is a high  $P_t$  direct photon production  $pp(\bar{p}) \rightarrow \gamma^{dir} + X$ . The region of high  $P_t$ , reached by UA1, UA2, CDF and D0 extends up to  $P_t \approx 60 GeV/c$  and recently up to  $P_t = 105 GeV/c$  [11]. These data together with the later ones and recent E706 and UA6 results give an opportunity for tuning the form of gluon distribution.

Here for the same aim we shall consider the process  $pp \rightarrow \gamma^{dir} + 1Jet + X$  defined in the leading order by two QCD subprocesses (12) and (13).

The “ $\gamma^{dir} + 1 Jet$ ” final state is more preferable than inclusive photon production  $\gamma + X$  from the viewpoint of extraction of information on gluon distribution. Indeed, in the case of inclusive direct photon production the cross section is given as an integral over partons distribution functions  $f_a(x_a, Q^2)$  ( $a = \text{quark or gluon}$ ), while in the case of  $pp \rightarrow \gamma^{dir} + 1 Jet + X$  for  $P_t^{Jet} \geq 30 GeV/c$  (i.e. in the region where “ $k_t$ ” smearing effects are not important) the cross section is expressed directly in terms of these distributions (see, for example, [12])

$$\frac{d\sigma}{d\eta_1 d\eta_2 dP_t^2} = \sum_{a,b} x_a f_a(x_a, Q^2) x_b f_b(x_b, Q^2) \frac{d\sigma}{dt}(a b \rightarrow 34) \quad (14)$$

where

$$x_{a,b} = P_t/\sqrt{s} \cdot (\exp(\pm\eta_1) + \exp(\pm\eta_2)). \quad (15)$$

We also used the following designations above:  $\eta_1 = \eta^\gamma$ ,  $\eta_2 = \eta^{Jet}$ ;  $P_t = P_t^\gamma$ ;  $a, b = q, \bar{q}, g$ ;  $3, 4 = q, \bar{q}, g, \gamma$ . Formula (14) and the knowledge of the results

of independent measurements of  $q, \bar{q}$  distributions allow the gluon  $f_g(x, Q^2)$  distribution to be determined after account of selection efficiencies of  $\gamma^{dir}$  candidates and the contribution of background, left after the used selection cuts (1–13 of Table 1), as it was discussed in Section 3 keeping in mind this task.

In the previous sections a lot of details connected with the structure and topology of these events and the objects appearing in them were discussed. Now with this information in mind we are in position to discuss application of the " $\gamma + Jet$ " event samples selected with the proposed cuts to estimate rates of gluon-based subprocess (12).

In Table 8 we present the  $Q^2 (\equiv (P_t^\gamma)^2)$  and  $x$  (defined according to (15)) distribution of the number of events that are caused by the  $q g \rightarrow \gamma + q$  subprocess, and passed cuts (1) – (7) of Section 2 ( $P_t^{out}$  was not limited):

$$P_t^\gamma > 40 \text{ GeV}/c, |\eta^\gamma| < 2.5, P_t^{Jet} > 30 \text{ GeV}/c, |\eta^{Jet}| < 5.0, P_t^{hadr} > 5 \text{ GeV}/c, \\ P_t^{isol} = 5 \text{ GeV}/c, \epsilon_{CUT}^\gamma = 7\%, \Delta\phi < 15^\circ, P_t^{clust} = 5 \text{ GeV}/c. \quad (16)$$

Table 8: Number of  $g q \rightarrow \gamma^{dir} + q$  events at different  $Q^2$  and  $x$  values for  $L_{int} = 20 \text{ fb}^{-1}$ .

$Q^2$ (GeV/c) <sup>2</sup>	$x$ values of a parton				All $x$
	$10^{-4}$ – $10^{-3}$	$10^{-3}$ – $10^{-2}$	$10^{-2}$ – $10^{-1}$	$10^{-1}$ – $10^0$	$10^{-4}$ – $10^0$
1600-2500	735.7	2319.2	2229.0	236.9	5521.0
2500-5000	301.6	1323.3	1402.7	207.4	3235.1
5000-10000	33.7	361.3	401.0	97.7	893.8
10000-20000	1.5	80.8	99.4	38.0	219.9
20000-40000	0	15.6	24.4	12.4	52.5
40000-80000	0	2.1	4.2	2.5	8.8

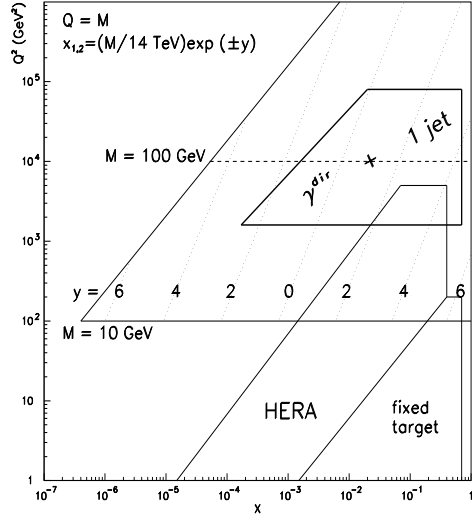
Table 9: Number of  $g c \rightarrow \gamma^{dir} + q$  events at different  $Q^2$  and  $x$  values for  $L_{int} = 20 \text{ fb}^{-1}$ .

$Q^2$ (GeV/c) <sup>2</sup>	$x$ values for $c$ -quark				All $x$
	$10^{-4}$ – $10^{-3}$	$10^{-3}$ – $10^{-2}$	$10^{-2}$ – $10^{-1}$	$10^{-1}$ – $10^0$	$10^{-4}$ – $10^0$
1600-2500	109.4	360.5	329.6	34.7	834.4
2500-5000	35.1	189.7	202.7	25.4	453.2
5000-10000	3.9	51.5	58.6	12.1	126.3
10000-20000	0.1	9.0	12.4	3.4	25.0
20000-40000	0	1.4	3.2	1.0	5.6
40000-80000	0	0.1	0.4	0.1	0.7

The analogous information for events with the charmed quarks in the initial state  $g c \rightarrow \gamma^{dir} + c$  is presented in Table 9. The simulation of the process

$g b \rightarrow \gamma^{dir} + b$  shows that the rates for the  $b$ -quark are 8 – 10 times smaller than for the  $c$ -quark.

Fig. 3 shows in the widely used  $(x, Q^2)$  kinematic plot what area can be covered by studying the process  $q g \rightarrow \gamma + q$ . The number of events in this area



is given in Table 8. From this figure and Table 8 it becomes clear that even at integrated luminosity  $L_{int} = 20 \text{ fb}^{-1}$  it would be possible to study the gluon distribution with good statistics of " $\gamma + Jet$ " events in the region of small  $x$  at  $Q^2$  about 2–3 orders of magnitude higher than now reached at HERA. It is worth emphasising that extension of the experimentally reachable region at the LHC to the region of lower  $Q^2$  overlapping with the area covered by HERA would also be of great interest.

Figure 3: The  $(x, Q^2)$  kinematic region for  $pp \rightarrow \gamma + Jet$  process.

## References

- [1] N.B. Skachkov, V.F. Konoplyanikov D.V. Bandourin, "Photon – jet events for calibration of HCAL". Second Annual RDMS CMS Collaboration Meeting. CMS Document 1996–213. CERN, December 16-17, 1996, p.7-23.
- [2] N.B. Skachkov, V.F. Konoplyanikov D.V. Bandourin, " $\gamma$ -direct + 1 jet events for HCAL calibration". Third Annual RDMS CMS Collaboration Meeting. CMS Document 1997–168. CERN, December 16-17, 1997, p.139-153.
- [3] D.V. Bandurin, V.F. Konoplyanikov, N.B. Skachkov, "Jet energy scale setting with " $\gamma$ +jet" events for a hadronic calorimeter of CMS." Fifth Annual RDMS CMS Collaboration Meeting. CMS Document 2000-058. Conference. "Physics Program with the CMS Detector", ITEP, Moscow, Russia. November 22-24, 2000. p. 422-427.

- [4] D.V. Bandourin, V.F. Konoplyanikov, N.B. Skachkov. “Jet energy scale setting with  $\gamma + Jet$ ” events at LHC energies.” JINR Preprints E2-2000-251 – E2-2000-255, JINR, Dubna, hep-ex/0011012, hep-ex/0011013, hep-ex/0011014, hep-ex/0011017, hep-ex/0011084.
- [5] D.V. Bandourin, V.F. Konoplyanikov, N.B. Skachkov, “  $\gamma + Jet$ ” events rate estimation for gluon distribution determination at LHC”, Part.Nucl.Lett.103:34-43,2000, hep-ex/0011015.
- [6] CMS Electromagnetic Calorimeter Project, Technical Design Report, CERN/LHCC 97–33, CMS TDR 4, CERN, 1997.
- [7] T. Sjostrand, Comp.Phys.Comm. **82** (1994)74.
- [8] S. Frixione, Phys.Lett. **B429** (1998)369.
- [9] S. Catani, M. Fontannaz and E. Pilon, Phys.Rev. **D58** (1998)094025.
- [10] P. Aurenche *et al.* Proc. of “ECFA LHC Workshop”, Aachen, Germany, 4-9 Oktob. 1990, edited by G. Jarlskog and D. Rein (CERN-Report No 90-10; Geneva, Switzerland 1990), Vol. **II**
- [11] D0 Collaboration, B. Abbott *et al.* , Phys.Rev.Lett. **84** 2786-2791,2000.
- [12] J.F. Owens, Rev.Mod.Phys. **59** (1987)465.

## Appendix

$$\hat{p}_\perp^{min} = 40 \text{ GeV}/c$$

$$P_t^{isol} < 2 \text{ GeV}/c, \quad \epsilon^{\tilde{\gamma}} < 5\%, \quad \Delta\phi = 15^\circ$$

Table 1: Number of events per  $L_{int} = 3 \text{ fb}^{-1}$

$P_{t \text{ cut}}^{clust}$ (GeV/c)	$P_{t \text{ cut}}^{out}$ (GeV/c)					
	5	10	15	20	30	1000
5	634000	1064000	1108000	1110000	1110000	1110000
10	1681000	3625000	4382000	4578000	4616000	4618000
15	1939000	4548000	6051000	6641000	6813000	6822000
20	2017000	4893000	6756000	7674000	8081000	8121000
30	2090000	5140000	7258000	8456000	9317000	9581000

Table 2:  $S/B$

$P_{t \text{ cut}}^{clust}$ (GeV/c)	$P_{t \text{ cut}}^{out}$ (GeV/c)					
	5	10	15	20	30	1000
5	$5.6 \pm 1.1$	$5.0 \pm 0.7$	$4.8 \pm 0.7$	$4.8 \pm 0.7$	$4.8 \pm 0.7$	$4.8 \pm 0.7$
10	$4.2 \pm 0.5$	$3.9 \pm 0.3$	$3.6 \pm 0.2$	$3.5 \pm 0.2$	$3.5 \pm 0.2$	$3.5 \pm 0.2$
15	$3.7 \pm 0.4$	$3.4 \pm 0.2$	$3.2 \pm 0.2$	$3.1 \pm 0.2$	$3.0 \pm 0.2$	$3.0 \pm 0.2$
20	$3.7 \pm 0.4$	$3.2 \pm 0.2$	$2.9 \pm 0.2$	$2.8 \pm 0.1$	$2.7 \pm 0.1$	$2.7 \pm 0.1$
30	$3.5 \pm 0.3$	$2.9 \pm 0.2$	$2.6 \pm 0.1$	$2.5 \pm 0.1$	$2.3 \pm 0.1$	$2.3 \pm 0.1$

Table 3:  $\langle F \rangle$ ,  $F = (P_t^\gamma - P_t^{Jet})/P_t^\gamma$

$P_{t \text{ cut}}^{clust}$ (GeV/c)	$P_{t \text{ cut}}^{out}$ (GeV/c)					
	5	10	15	20	30	1000
5	0.008	0.008	0.008	0.008	0.008	0.008
10	0.003	0.009	0.013	0.013	0.013	0.013
15	0.005	0.011	0.018	0.019	0.022	0.022
20	0.006	0.012	0.020	0.023	0.026	0.027
30	0.005	0.012	0.021	0.024	0.029	0.030

Table 4:  $\sigma(F)$ ,  $F = (P_t^\gamma - P_t^{Jet})/P_t^\gamma$

$P_{t \text{ cut}}^{clust}$ (GeV/c)	$P_{t \text{ cut}}^{out}$ (GeV/c)					
	5	10	15	20	30	1000
5	0.063	0.075	0.079	0.079	0.079	0.079
10	0.068	0.085	0.097	0.102	0.104	0.104
15	0.070	0.090	0.109	0.123	0.129	0.130
20	0.070	0.092	0.113	0.133	0.145	0.147
30	0.071	0.093	0.117	0.140	0.159	0.163



$$\hat{p}_{\perp}^{min} = 200 \text{ GeV}/c$$

$$P_t^{isol} < 2 \text{ GeV}/c, \quad \epsilon^{\tilde{\gamma}} < 5\%, \quad \Delta\phi = 15^{\circ}$$

Table 5: Number of events per  $L_{int} = 3 \text{ fb}^{-1}$

$P_{t \text{ cut}}^{clust}$ (GeV/c)	$P_{t \text{ cut}}^{out}$ (GeV/c)					
	5	10	15	20	30	1000
5	620	1220	1330	1360	1360	1380
10	1660	4100	5220	5700	5820	5840
15	2080	5420	7880	9310	10160	10290
20	2230	5960	9020	11240	13230	13840
30	2310	6290	9770	12590	16570	19510

Table 6:  $S/B$

$P_{t \text{ cut}}^{clust}$ (GeV/c)	$P_{t \text{ cut}}^{out}$ (GeV/c)					
	5	10	15	20	30	1000
5	179 $\pm$ 165	114 $\pm$ 61	102 $\pm$ 49	104 $\pm$ 50	104 $\pm$ 50	104 $\pm$ 50
10	48.9 $\pm$ 12.4	48.4 $\pm$ 8.6	47.2 $\pm$ 7.6	45.7 $\pm$ 6.0	45.5 $\pm$ 6.1	45.5 $\pm$ 6.1
15	42.1 $\pm$ 11.2	42.8 $\pm$ 7.1	39.9 $\pm$ 5.3	31.5 $\pm$ 3.5	28.4 $\pm$ 2.9	28.3 $\pm$ 2.9
20	31.2 $\pm$ 7.0	36.1 $\pm$ 5.3	29.7 $\pm$ 3.3	24.7 $\pm$ 2.3	20.7 $\pm$ 1.6	19.4 $\pm$ 1.5
30	30.2 $\pm$ 6.6	28.6 $\pm$ 3.7	23.2 $\pm$ 2.2	19.3 $\pm$ 1.5	15.8 $\pm$ 1.0	13.6 $\pm$ 0.8

Table 7:  $\langle F \rangle$ ,  $F = (P_t^{\gamma} - P_t^{Jet})/P_t^{\gamma}$

(GeV/c)	5	10	15	20	30	1000
5	0.003	0.002	0.003	0.003	0.003	0.004
10	0.001	0.003	0.004	0.005	0.005	0.005
15	0.001	0.003	0.005	0.007	0.007	0.008
20	0.001	0.003	0.005	0.007	0.008	0.009
30	0.001	0.003	0.005	0.007	0.009	0.014

Table 8:  $\sigma(F)$ ,  $F = (P_t^{\gamma} - P_t^{Jet})/P_t^{\gamma}$

$P_{t \text{ cut}}^{clust}$ (GeV/c)	$P_{t \text{ cut}}^{out}$ (GeV/c)					
	5	10	15	20	30	1000
5	0.014	0.017	0.019	0.020	0.022	0.024
10	0.015	0.019	0.023	0.025	0.027	0.027
15	0.015	0.020	0.025	0.029	0.033	0.035
20	0.015	0.021	0.026	0.031	0.038	0.042
30	0.015	0.021	0.027	0.033	0.043	0.054